Progress in Organic Coatings 84 (2015) 143–152

Contents lists available at ScienceDirect

Progress in Organic Coatings

journal homepage: www.elsevier.com/locate/porgcoat

Influence of the coating method on the formation of superhydrophobic silicone–urea surfaces modified with fumed silica nanoparticles

Cagla Kosak Söz, Emel Yilgör, Iskender Yilgör*

KUYTAM Surface Science and Technology Center, Chemistry Department, Koc University, Istanbul, Turkey

ARTICLE INFO

Article history:
Received 18 December 2014
Received in revised form 10 March 2015
Accepted 11 March 2015
Available online 7 April 2015

Keywords:
Superhydrophobic surfaces
Fumed silica
Spray coating
Spin coating

ABSTRACT

Effect of the coating method on the formation of superhydrophobic polydimethylsiloxane–urea copolymer (TPSC) surfaces, modified by the incorporation of hydrophobic fumed silica nanoparticles was investigated. Four different coating methods employed were: (i) layer-by-layer spin-coating of hydrophobic fumed silica dispersed in an organic solvent onto TPSC films, (ii) spin-coating of silica–polymer mixture onto a glass substrate, (iii) spray coating of silica/polymer mixture by an air-brush onto a glass substrate, and (iv) direct coating of silica–polymer mixture by a doctor blade onto a glass substrate. Influence of the coating method, composition of the polymer/silica mixture and the number of silica layers applied on the topography and wetting behavior of the surfaces were determined. Surfaces obtained were characterized by scanning electron microscopy (SEM), white light interferometry (WLI) and advancing and receding water contact angle measurements. It was demonstrated that superhydrophobic surfaces could be obtained by all methods. Surfaces obtained displayed hierarchical micro-nano structures and superhydrophobic behavior with static and advancing water contact angles well above 150° and fairly low contact angle hysteresis values.

1. Introduction

Preparation and characterization of superhydrophobic polymeric surfaces and coatings have been investigated extensively during the past 15 years, following the detailed description of the surface structures and hierarchical micro and nano topographies of a large number of natural plant leaves [1,2]. A major reason for such a remarkable interest in superhydrophobic coatings and surfaces has been their interesting combination of properties, such as the self-cleaning, anti-fouling, stain-resistant and ice-repellant behaviors [3–5], which enable potential applications in a variety of fields, which include paints and coatings, textiles, exterior glass windows, rooftops, windshields, solar panels, aircraft wings and wind turbine blades [3,4,6,7]. As well documented in the literature, wetting behavior of a surface is mainly controlled by two parameters, which are; (i) the surface chemical structure and composition, and (ii) the surface topography or roughness [8–10]. When naturally occurring superhydrophobic plant surfaces, such as a lotus leaf surface is examined under a scanning electron microscope, it is seen that the surface is covered by irregularly distributed, micron-sized protrusions called *papilla*, which also display a fury nanoscale roughness [1,2,10]. When such a micro-nano dual surface roughness is combined with the inherent hydrophobicity of the waxy layer on the leaf, they provide the lotus leaf its superhydrophobicity, with static water contact angle values above 150° and contact angle hysteresis values below 10° [11–17]. Similar superhydrophobic surfaces with micro-nano hierarchical structures are also observed in various insects, such as the butterfly wings, which display two key periodic structures [18–21]. The individual shingle-like epidermal scales which comprise the wings of butterflies are about 40 × 80 μm each and the micro-relief of the raised ridges covering each wing scale, each between 1.0 and 1.5 μm [22]. The contact angles of the water droplets on the butterfly wing surface are measured to be higher than 150° [23], which rolls freely when the inclining angle is larger than 3°, thus keeping the butterfly wing surface clean of dust and other debris. A wide range of synthetic materials with superhydrophobic surfaces, based on polymers, ceramics, metals or hybrid composite systems have been prepared by templating the natural systems such as lotus leaf, rice leaf, butterfly wings [18,19] and others [24,25].

Theoretical treatment of the effect of the topography on the wetting behavior of surfaces has been provided by Wenzel [26]

* Corresponding author. Tel.: +90 212 338 1418; fax: +90 212 338 1559.
E-mail address: iyilgor@ku.edu.tr (I. Yilgör).

http://dx.doi.org/10.1016/j.porgcoat.2015.03.015
0300-9440/

and Cassie and Baxter [27]. Wenzel assumed complete wetting of a rough surface by the droplet and modified the contact angle measured by introducing a roughness factor (r), defined as the ratio of the actual area of a rough surface to its projected geometric area, which has a value greater than 1. Cassie and Baxter assumed the apparent contact angle on a rough surface to be the weighted average of the contact angles on the solid and air surfaces. They defined (f) to be the surface fraction on top of the protrusions and ($1-f$) on air pockets [28]. When Cassie–Baxter and Wenzel relationships are combined, a general equation given below, which provides the apparent contact angles measured on a rough surface (θ_R) as a function of the contact angle measured on a smooth surface (θ), roughness (r) and surface void fraction (f) is obtained. This equation clearly indicates that for an inherently hydrophobic and flat surface with a contact angle greater than 90°, increased surface roughness will lead to much higher contact angles. Modified versions of this equation explaining the contact angle behavior of rough surfaces have also been reported [29–32].

$$\cos\theta_R = r \cdot f \cdot \cos\theta + f - 1$$

As a result of the remarkable academic and industrial interest in the superhydrophobicity, a large number of methods and processes have been developed for the preparation of superhydrophobic polymer surfaces showing hierarchical micro/nano roughnesses. These include layer-by-layer deposition [33], electrospinning [34], microphase separation [28,35,36], etching [37,38], spin-coating or dip-coating [28,39,40], sol–gel synthesis [10,41], templating [20,21,28,36,42], spraying [5,43] and many others [10,16,28,37,38,44]. Although a wide range of approaches have been proposed for the preparation of superhydrophobic polymer surfaces, most of them are polymer specific, fairly complex and involve several steps. Recently we reported a fairly simple method, which was based on the spin coating of fumed silica dispersions in an organic solvent onto polymer surfaces for the preparation of polymeric materials with controlled wettability, from superhydrophilic to superhydrophobic [39,40]. The method was applicable to a wide range of polymeric materials, thermoplastic or thermoset.

In this study we investigated the utilization of more practical coating methods for the preparation of superhydrophobic silicone–urea copolymer surfaces, which included spray coating using an airbrush and direct coating using a doctor blade, in addition to the spin-coating process. Topography and the average roughness of the superhydrophobic polymer surfaces obtained were characterized by field emission scanning electron microscopy (FESEM) and white light interferometry (WLI). Static, advancing and receding water contact angle (CA) measurements were also performed to demonstrate the formation of superhydrophobic surfaces. Our results indicate that: (i) the extent of surface silica coverage and the distance between silica particles, (ii) average sizes of the silica particles or agglomerates, (iii) presence of micro-nano hierarchical structures, and (iv) the average surface roughness, play critical roles in obtaining superhydrophobic surfaces.

2. Experimental

2.1. Materials

Segmented thermoplastic polydimethylsiloxane-urea copolymer (Geniomer TPSC 140) (TPSC) with a PDMS content of about 92% by weight and the hydrophobic fumed silica (HDK H2000) were supplied by Wacker Chemie, Munich, Germany [45]. Primary particle size for the hydrophobic silica is reported to be 5–30 nm, which increases to 100–250 nm after aggregation. The specific surface area is 170–230 m^2/g [45]. Reagent grade isopropanol (IPA), tetrahydrofuran (THF) and toluene were obtained from Merck and were used as received.

2.2. Preparation of superhydrophobic silicone–urea copolymer surfaces

Methods used for the preparation of superhydrophobic polymer surfaces through the use of hydrophobic fumed silica (HDK H2000) are explained in detail below.

2.2.1. Spin coating of silica dispersed in THF onto the TPSC surface

The first method was layer-by-layer spin coating of silica particles onto TPSC surface from a dispersion in THF, which was explained in detail previously [39,40]. TPSC was dissolved in IPA (15% by weight), whereas the hydrophobic silica was dispersed in THF at a concentration of 0.5% by weight and was subjected to ultrasound sonication at a frequency of 35 kHz on a Sonorex RK 255H type bath for 10 h. Dynamic light scattering (DLS) measurements on hydrophobic silica suspensions in THF (10 mg/mL) indicated fairly homogeneous distribution of the silica nanoparticles, with a number average size distribution of 44 ± 9 nm. Spin coating was applied on a Model 7600 Spin Coater by Specialty Coating Systems, Inc., Indianapolis, IN, USA.

Glass slides ($20 \times 20 \times 0.15$ mm), cleaned by wiping with IPA and THF were used as the substrate for spin coated TPSC films, which had a thickness of about 20–30 μm. 8–10 drops of 0.5% by weight silica dispersion in THF were then placed onto the polymer film and spin coated after waiting for 1 min to allow the surface wetting and efficient penetration of silica particles into the polymer film. This step was repeated several times to achieve optimum coverage. To improve the durability, the silica containing surfaces were finally spin coated with a thin layer of TPSC film. Spin coating was performed at 1000 rpm for 70 s. All samples were dried at room temperature overnight and then in a vacuum oven at room temperature until constant weight and were kept in sealed containers until further testing.

2.2.2. Spin coating of TPSC/silica dispersions on a glass substrate

TPSC was dissolved in IPA at a concentration of 0.5% by weight. To this polymer solution silica particles were added at different amounts to obtain TPSC/silica ratios of 1/4, 1/7 and 1/10 (by weight). Mixtures were stirred vigorously for 30 min by a magnetic stirrer and then were sonicated for 30 min to obtain homogeneous dispersions. DLS measurements on TPSC/silica (1/10) mixtures containing 40 mg/mL silica indicated number average particle size distribution of 272.0 ± 24.7 nm, which was stable for several hours. TPSC/silica dispersions were spin coated onto glass slides at 1000 rpm. Spin coating step was repeated to apply successive layers. Samples were dried at room temperature overnight and then in a vacuum oven at 40 °C for 24 h.

2.2.3. Coating of TPSC/silica dispersions on a glass substrate using a doctor blade

TPSC/silica (1/10) (by weight) dispersion prepared in IPA as described before was coated on a glass substrate using a doctor blade with a gauge thickness of 200 μm. Coating was dried overnight at room temperature and then in a vacuum oven at 40 °C for 24 h.

2.2.4. Spray coating of TPSC/silica dispersions with an airbrush

Spray coating was applied by using a Max H2000 model Cora airbrush painter with a nozzle diameter of 0.8 mm, pressurized by a Black and Decker compressor. TPSC/silica (1/10) (by weight) mixture prepared in IPA was transferred into the tank of the airbrush and the mixture was sprayed onto the glass slides under different conditions. The coating parameters included the tank pressure,

distance between nozzle and the substrate and the duration of the spraying process.

2.3. Characterization methods

Dynamic light scattering (DLS) measurements on silica dispersions were performed on Malvern ZetaSizer Nano-S Instrument with the Nano-S software. Glass cuvettes with square apertures were used as sample holders. Transparencies of the samples were determined in the visible region, using a Schimadzu Model 3600 UV–vis-NIR spectrophotometer against air as the reference.

Static water contact angle measurements were conducted at room temperature ($23 \pm 2\,^{\circ}C$) on a Dataphysics OCA 35 goniometer equipped with SCA 20 software, which provided the electronic control of the device parameters and measurement of the contact angles. An average of at least 10 contact angle readings were taken for each sample using 5 μL deionized, triple distilled water droplets. Contact angle hysteresis measurements were conducted by dynamic sessile drop method by placing a 0.5 μL water droplet onto the surface from syringe tip and gradually increasing to 5 μL. During the measurement of the advancing angle, the volume of the sessile drop was increased from 5 μL to 25 μL at a rate of 0.2 mL/s and the highest angle achieved was accepted as the advancing angle. Then, the volume of the water droplet was decreased from 25 μL to 5 μL with the same rate. The lowest angle was accepted as the receding contact angle after the contact line between the water droplet and the surface started to decrease with a satisfactory drop shape.

A field-emission scanning electron microscope (FESEM) (Zeiss Ultra Plus Scanning Electron Microscope) operated at 2–10 kV was used to investigate the coated surfaces. Prior to FESEM study, samples were coated with a 2–3 nm layer of gold to minimize charging. Surface topographies and average roughness values of the silica coated surfaces were investigated by White Light Interferometry (WLI) on a Bruker Contour GT Motion 3D Microscope and Non Contact Surface Profiler at the vertical scanning interferometry (VSI) mode. Using WLI feature sizes from sub nanometer to millimeter range can easily be measured. In VSI mode average surface roughnesses with height discontinuities between 150 nm and several mm can be precisely determined. At least 10 surface maps with dimensions of $47 \times 63\ \mu m^2$ were obtained from different parts on the sample to calculate the average roughness values.

3. Results and discussion

Although the superhydrophobic behavior of rough surfaces have been theoretically formulated by Wenzel [26] and Cassie and Baxter [27] over 70 years ago, preparation, characterization and applications of superhydrophobic surfaces have received widespread attention only during the past 10–15 years following several publications reporting the characteristic surface morphologies and superhydrophobic properties of a large number of plants [1,2]. As a classical example, the surface of the lotus leaf was found to be consisting of cone type protrusions with base diameters of 5–15 μm, heights of 10–50 μm and aspect ratios in 0.7–10 range. They are irregularly distributed on the leaf surface with distances between each other ranging from 10 to 100 μm. The cones also displayed nanometer sized hairy features, which are reported to be critical in achieving superhydrophobic surfaces with low contact angle hysteresis [11–17]. Some of the pioneering work in the field was performed by McCarthy and co-workers [8,9,11–14,46–58] and other groups [4,10,15–17,28,41,59–74], which included experimental studies on the preparation and characterization of superhydrophobic surfaces and critical evaluation of the theoretical foundations. A large number of excellent review articles were also published recently, which provide detailed experimental and theoretical information on various aspects of superhydrophobic surfaces [4,10,28,36–38,44,62,63,75].

In this report we discuss our studies on the development of superhydrophobic silicone–urea copolymer surfaces by using hydrophobic fumed silica and various coating techniques. Effect of; (i) the coating method, (ii) TPSC/silica ratio in the coating mixture and (iii) the number of silica layers applied, on the formation of the superhydrophobic surfaces were investigated. Surface topographies, including the extent of surface coverage by silica particles, their size, distribution and average surface roughness values were determined by various techniques. Formation of superhydrophobic surfaces was demonstrated by advancing and receding water contact angle measurements and contact angle hysteresis (CAH). Before beginning our discussions, it is important to note that virgin TPSC coated surfaces display a static water contact angle of $110.0 \pm 1.0^{\circ}$ and contact angle hysteresis of $22.0 \pm 2.0^{\circ}$, fairly similar to that of the crosslinked silicone rubber. These values are independent of the coating method used.

3.1. Spin coating of silica dispersed in THF onto the TPSC surface

Surface modification of TPSC through layer-by-layer spin coating by using a silica dispersion in THF has already been discussed in detail in our previous publications [39,40,76]. As a result here we will only provide examples regarding the topography, average roughness and water contact angle behavior of the surfaces obtained by this technique as a reference in order to compare them with the topography and properties of the surfaces obtained by other coating techniques. Fig. 1a–c provides the SEM images of the TPSC surfaces spin coated with different number of layers of hydrophobic fumed silica. Since very dilute silica dispersion (0.5% by weight in THF) is used, surface coverage of particles and surface roughness increase slowly as can be seen through Fig. 1a–c. TPSC surface becomes superhydrophobic after three layers of coating as indicated by the values of the static water contact angles displayed on Fig. 1a–c [76]. Average surface roughness of the virgin TPSC coating is 6.3 ± 1.1 nm, whereas the roughness values for samples coated with one, three and seven layers of silica are 76.6 ± 14.4, 124.3 ± 28.6 and 208.0 ± 70.4 nm, respectively [76].

3.2. Spin coating of TPSC/silica dispersions on a glass substrate

In order to simplify the process and obtain robust, superhydrophobic surfaces after minimum number of coating layers and possibly with only one layer, in this process silica particles are premixed with the silicone–urea copolymer in dilute IPA solutions (2–5% by weight solids) to obtain TPSC/silica ratios of 1/4, 1/7 and 1/10 (by weight). Solutions were then spin coated on glass substrates, to obtain films with thicknesses in 20–30 μm range. SEM images of TPSC/silica (1/10) coated glass surfaces as a function of the number of layers of coating applied are reproduced in Fig. 2. Due to the higher concentration of the silica dispersion used, after only one layer of coating the surfaces obtained displayed fairly homogeneous and dense silica coverage and superhydrophobic properties with contact angles well above 160° as displayed on each SEM image. As expected, application of successive layers of coatings increased the density of the surface silica coverage. Average sizes of the agglomerated silica particles also increased slightly. As shown in Fig. 3 silica agglomerates displayed nanoroughness and all surfaces were highly superhydrophobic with very small contact angle hysteresis values as shown on Table 1.

Two-dimensional surface topography images and average surface roughness values of silica coated TPSC surfaces were obtained using a White Light Interferometer (WLI). WLI images of the surfaces spin coated with silica are provided in Fig. 4a and b and

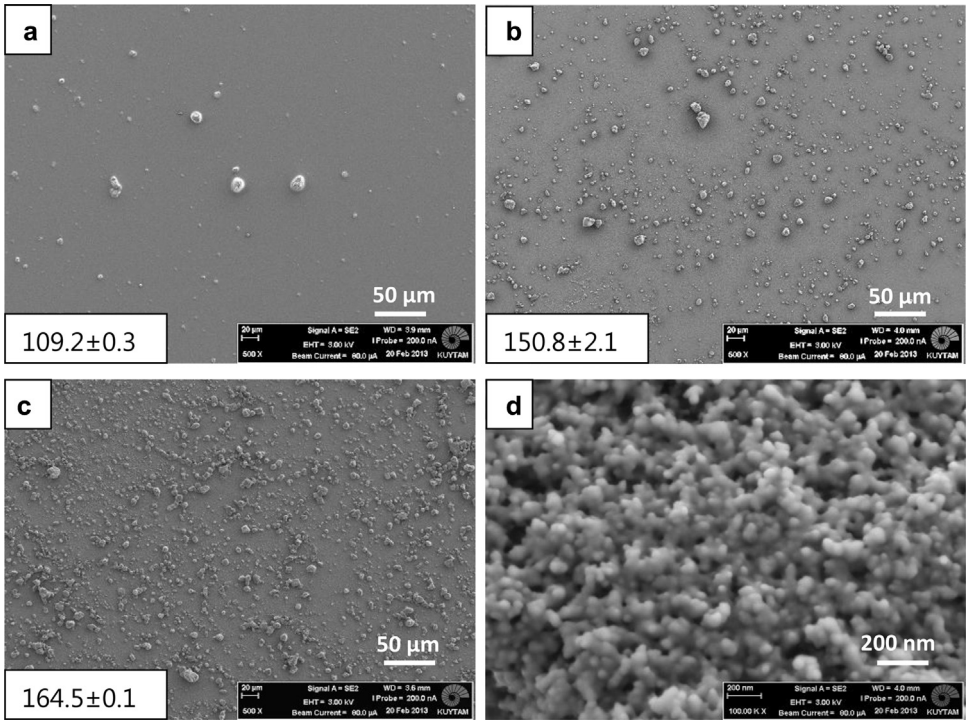

Fig. 1. SEM images of hydrophobic fumed silica coated TPSC surfaces, (a) one layer, (b) three layers and (c) seven layers of silica and (d) expanded wiev of an agglomerated micron sized silica particle displaying nanostructure.

roughness profiles along *X* and *Y* axes are given in Fig. 4c and d. Average heights of silica agglomerates were generally around 1–2 μm with maximum heights reaching to about 4 μm as shown in Fig. 4c and d.

Table 1 provides the average surface roughness values and static water contact angles as a function of the TPSC/silica ratio and the number of coating layers applied. As can easily be seen from Table 1, even after one layer of coating with (1/4) mixture, a surface with an average roughness value above 100 nm is obtained, which is around the threshold roughness value to obtain a superhydrophobic surface based on our previous studies for the TPSC system [76]. As summarized on Table 1, as the TPSC/silica ratio in the coating

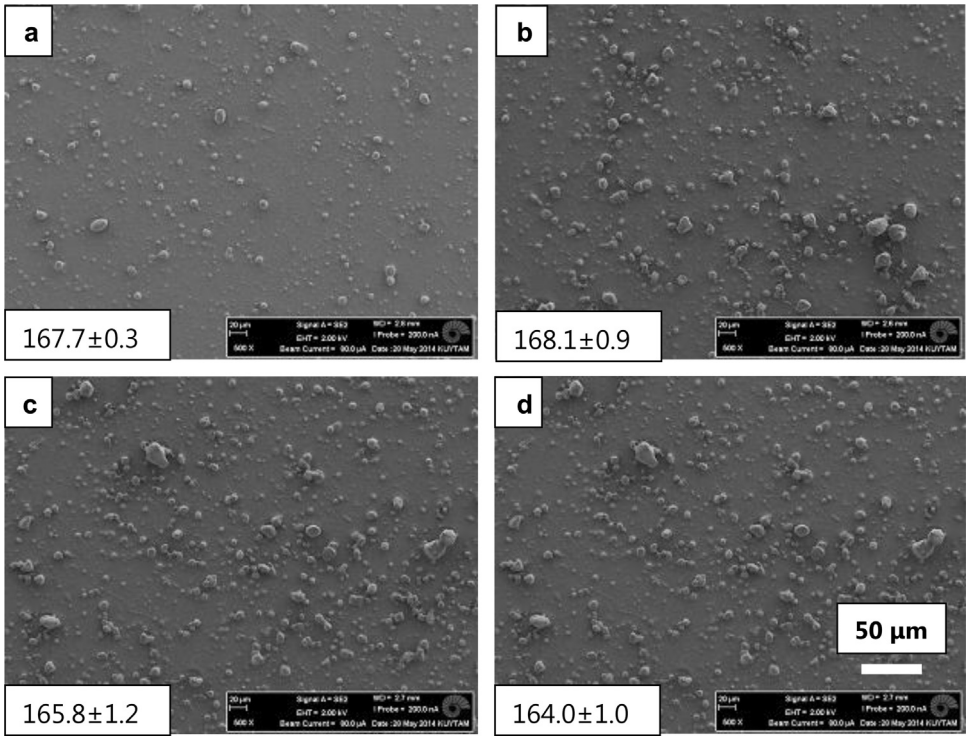

Fig. 2. SEM images of TPSC/silica (1/10) spin-coated glass surfaces, (a) one layer, (b) two layers, (c) three layers and (d) four layers of spin-coatings. Scale bar is 50 μm for all samples.

Table 1
Average surface roughness values and static water contact angles as a function of the TPSC/Silica ratio (by weight) and number of coating layers applied.

	TPSC/Silica: 1/4		TPSC/Silica: 1/7			TPSC/Silica: 1/10		
	R_a (nm)	CA (°)	R_a (nm)	CA (°)	CAH (°)	R_a (nm)	CA (°)	CAH (°)
One layer	127 ± 34	144.5 ± 1.1	140 ± 31	168.0 ± 0.7	6.6	195 ± 72	167.7 ± 0.3	7.0
Two layers	142 ± 72	163.4 ± 0.4	172 ± 8	168.1 ± 1.1	2.4	222 ± 110	168.1 ± 0.9	3.0
Three layers	141 ± 64	165.0 ± 0.8	190 ± 29	167.4 ± 1.5	2.1	207 ± 45	165.8 ± 1.2	2.1
Four layers	178 ± 42	167.5 ± 0.9	189 ± 38	169.7 ± 0.8	4.3	237 ± 40	164.0 ± 1.0	2.4

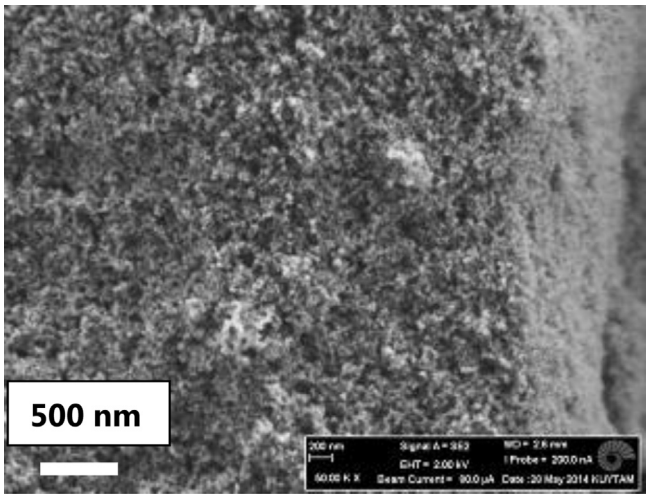

Fig. 3. SEM image of the nanostructure displayed by the silica agglomerates on three layers of TPSC/silica (1/10) spin coated glass surface.

solution increases to (1/7) and (1/10) or the number of coating layers applied is increased, the average roughness values obtained also increase, as expected. Except for the surface obtained by a single layer coating of the (1/4) mixture, which displayed a static water contact angle of 144.5°, all surfaces displayed very high water contact angles between 163 and 170° and water contact angle hysteresis values well below 10°, clearly indicating the formation of superhydrophobic surfaces.

3.3. Coating of TPSC/silica dispersions on a glass substrate using a doctor blade

Conventionally, doctor blade technique has been an important method for the preparation of thin polymeric films and coatings on various substrates from solution. It is a fairly simple technique and provides precise control of the film thickness and is widely used both for research and commercial applications, especially for the direct or transfer coating of woven and non-woven fabrics.

In this study a TPSC/silica (1/10) mixture was prepared in IPA and was coated on a clean glass surface using a doctor blade with a gap thickness of 200 μm, which provided a dry coating thickness of about 5 μm. SEM images of the coated surfaces are provided in Fig. 5 at various magnifications to provide the details of the topography and the hierarchical micro-nano structures obtained. Fig. 5a clearly shows very homogeneous distribution of the silica particles on the surface with particle sizes ranging in a fairly narrow range of about 2–5 μm, as shown on Fig. 5b. Silica particles are well embedded into the polymer (Fig. 5c), providing a robust and durable surface. The surface of the silica particles clearly displays

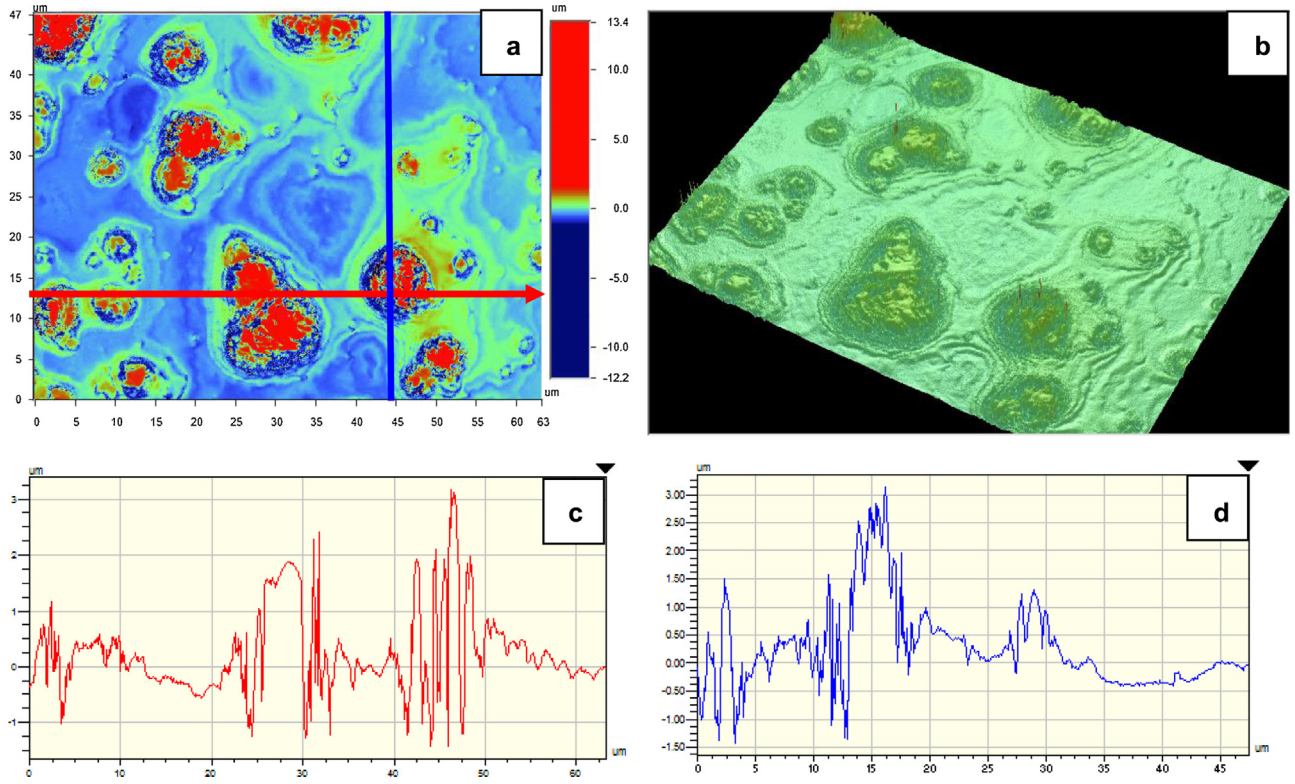

Fig. 4. 47 × 63 μm² (a) 2D and (b) 3D WLI images of three layers of TPSC/silica (1/10) spin coated glass surface and the roughness profiles along (c) *X* and (d) *Y* axes.

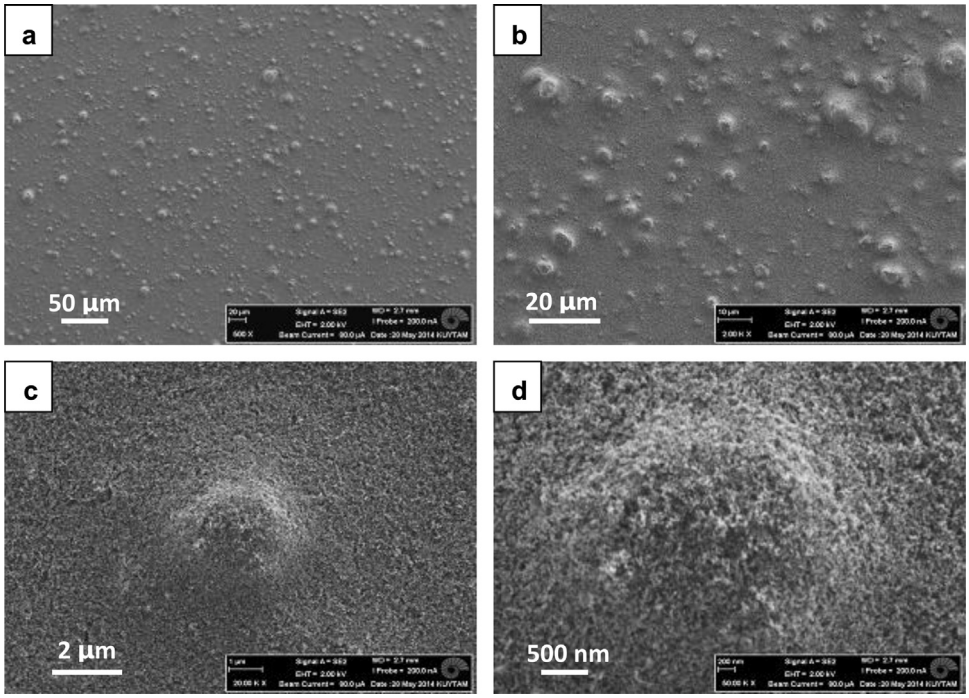

Fig. 5. Surface SEM images of the doctor blade coated TPSC/silica films at various magnifications providing the details of the topography and micro-nano structures formed. (a) 500×, (b) 2000×, (c) 20,000× and (d) 50,000×.

a hairy nanostructure (Fig. 5d), similar to the lotus leaf or other natural surfaces.

WLI image of the film surface is provided in Fig. 6a, together with the roughness profiles along *X* (Fig. 6b) and *Y* (Fig. 6c) axes. In addition to a fairly narrow particle size and homogeneous distribution, average heights of the silica agglomerates are also in a very narrow range around 1–2 μm. Average surface roughness (R_a) was determined to be 168 ± 57 nm by WLI studies. Formation of a superhydrophobic surface was demonstrated by a static water contact angle of 161.0 ± 1.2° and a contact angle hysteresis value below 10°.

3.4. Spray coating of TPSC/silica dispersions with an airbrush

Spray coating is one of the most versatile and practical coating methods, which can be used on small or large areas and on flat or intricate surfaces successfully. In this study we utilized TPSC/silica (1/10) dispersion in IPA and spray coated 2 × 2 cm^2 glass slides. During the coating process we investigated the influence of pressure, distance between nozzle and substrate and spray time on the extent of surface silica coverage, topography, average roughness and static water contact angles and contact angle hysteresis of the surfaces obtained. All of the samples discussed here were prepared using a tank pressure of 2 bar and nozzle to sample distance of 20 cm. The only variable was the spray time, which was 1, 2 and 3 s. SEM images of silica modified TPSC surfaces obtained at different spray times are reproduced in Fig. 7.

SEM images provided in Fig. 7 clearly indicate a fairly homogeneous coverage of the TPSC surfaces with silica aggregates, regardless of the spray time. Coating thickness obtained for 2 s spray time is about 35 μm. Average diameters of the silica aggregates are generally in 2–20 μm range. As the spray time increases there seem to be a slight increase in the average particle size. More interestingly the average distance between silica agglomerates seem to decrease with an increase in the spray time. As will be discussed later on in detail, this seems to have a significant effect on the contact angle hysteresis behavior of the surfaces. For a better understanding of the nature of the surface structures formed, higher magnification SEM images of the sample coated for 2 s are provided in Fig. 8. As can be seen in Fig. 8a, silica agglomerates are homogeneously distributed and well embedded into the polymer matrix, indicating the formation of a durable surface. The distance between silica aggregates seem to be between 1 and 20 μm. When closely examined, the hairy surface nanostructure of the silica particles can also clearly be seen, as provided in Fig. 8b. This clearly demonstrates the formation of a hierarchical surface structure with micro-nano features, which was shown to be critical in obtaining superhydrophobic behavior [1,2,10].

2D and 3D WLI images and roughness profiles of the surface obtained for 2 s spray coated sample are reproduced in Fig. 9. 47 × 63 μm^2 2D and 3D images given in Fig. 9a and b show a fairly good surface coverage and a broad distribution of silica agglomerates with particle sizes in 2–20 μm range. Heights of the large silica agglomerates are around 5 μm, which are much higher than those obtained by doctor blade coating technique. Formation of such large silica agglomerates results in an increase in the average surface roughness from about 170 nm for the doctor blade coated sample to above 300 nm for the spray coated samples as given in Table 2. Interestingly, the roughness profiles of the 47 × 63 μm^2 surface provided in Fig. 9c and d clearly shows the presence of fairly smooth valleys between silica agglomerates.

Table 2 provides a summary of the effect of spray time on the average surface roughness, static water contact angles and contact angle hysteresis (CAH) for TPSC/silica (1/10) coatings performed under a pressure of 2 bar and at a nozzle to substrate distance of 20 cm.

As provided in Table 2, all samples display average surface roughness values between 300 and 400 nm, which is fairly high. Average surface roughness values of the samples show a significant increase with spray time, which may be expected. As can clearly be seen in Table 2, all surfaces display very high static water contact angles above 160°, indicating the formation of superhydrophobic surfaces. Contact angle hysteresis (CAH) values for samples S2 and S3 are 4.8 and 2.9° respectively, strongly supporting the formation

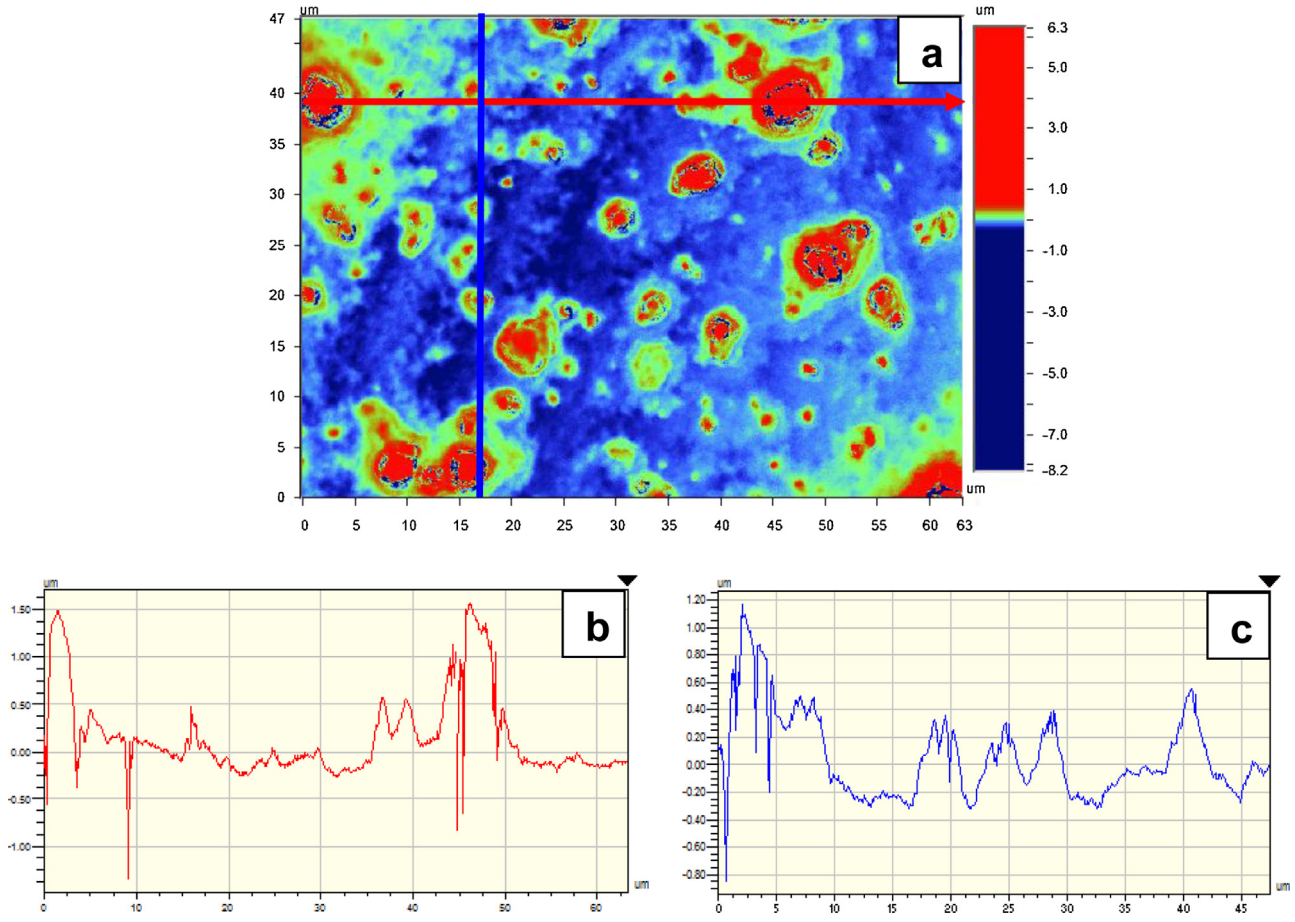

Fig. 6. 47 × 63 μm² WLI image of (a) the doctor blade coated TPSC/silica (1/10) surface and the roughness profiles along (b) *X* and (c) *Y* axes.

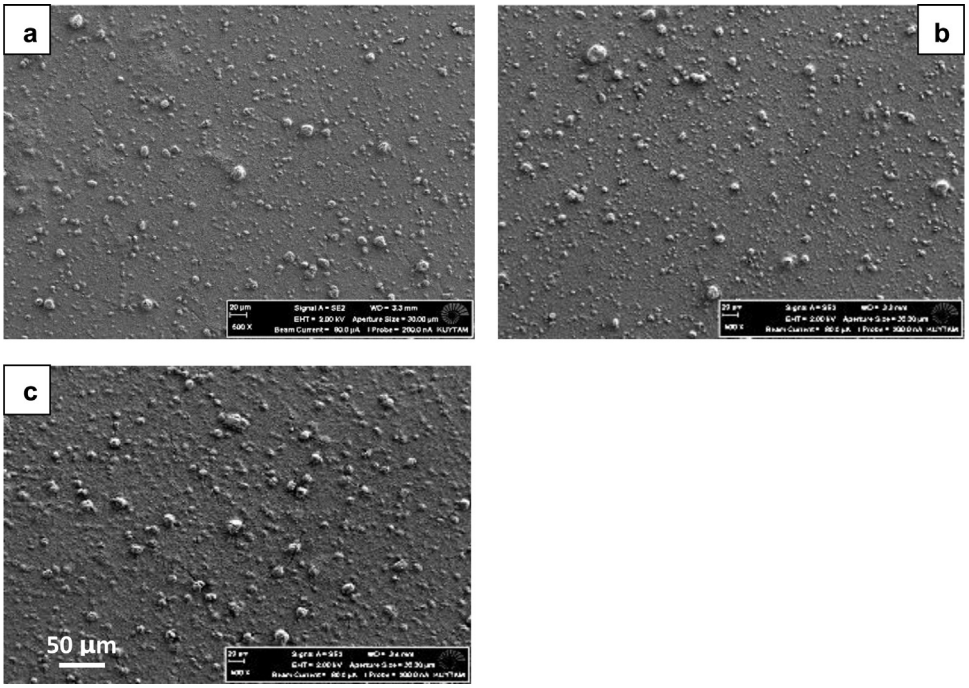

Fig. 7. SEM images of spray coated TPSC/silica (1/10) surfaces. (a) 1 s, (b) 2 s, and (c) 3 s. Scale bar is the same for all samples.

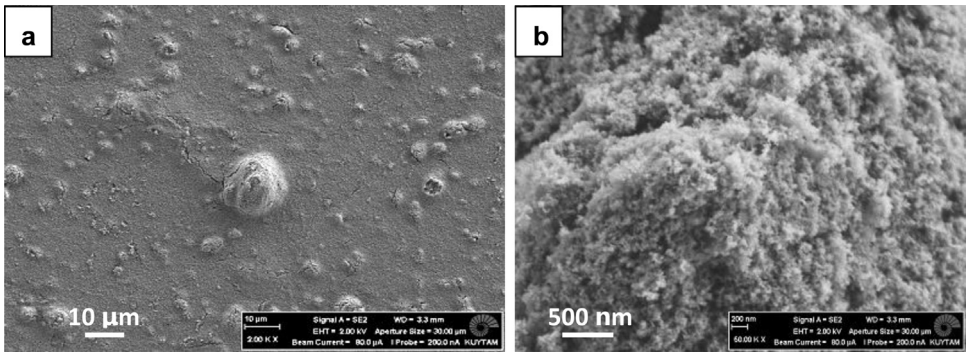

Fig. 8. Surface SEM images of the TPSC/silica (1/10) sample spray coated for 2 s, showing the formation of micro-nano hierarchical surface structures.

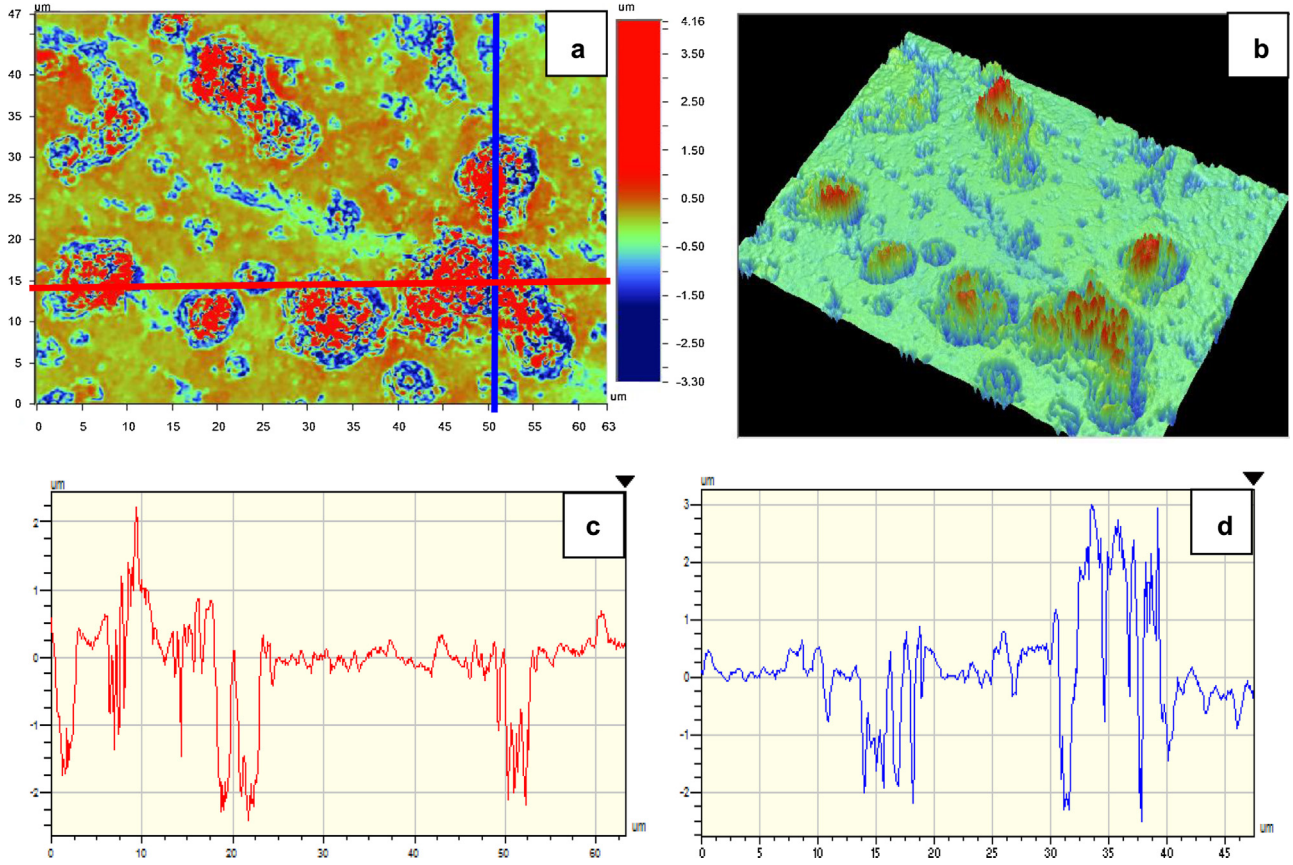

Fig. 9. (a) 2D and (b) 3D 47 × 63 μm^2 WLI images of the 2 s TPSC/silica (1/10) spray coated sample surface and the roughness profiles along (c) *X* and (d) *Y* axes.

of truly superhydrophobic surfaces. Interestingly, although the static water contact angle for sample S1 is above 160°, its CAH value is 26° and very high. When the SEM images provided in Fig. 7 is closely examined we believe this is mainly due to the presence of a large number of smaller sized silica agglomerates on sample S1 surface, together with the longer distances between the agglomerates. We believe the smaller silica agglomerates separated from each other by longer distances are not able to hold the water droplets on the top of the protrusions with an air cushion under them as in the case of Cassie–Baxter regime schematically shown in Fig. 10a. As the droplets get larger during CAH measurements, they seem to penetrate through the agglomerates and wet the surface, thereby changing the mechanism from Cassie–Baxter to the Wenzel regime (Fig. 10b), which results in a decrease in the receding water contact angle and an increase in the CAH. Detailed studies in order to better understand this behavior is underway. In

Table 2
Effect of spray time on the average surface roughness, static water contact angles and contact angle hysteresis values on spray coated TPSC/silica surfaces performed under 2 bar pressure and at a nozzle to substrate distance of 20 cm.

Sample no	Pressure (bar)	Spray time (s)	Distance (cm)	Roughness (R_a) (nm)	Av. CA (°)	CAH (°)
S1	2	1	20	293 ± 85	162.0 ± 1.8	26
S2	2	2	20	375 ± 59	165.7 ± 0.5	4.8
S3	2	3	20	410 ± 107	162.2 ± 0.1	2.9

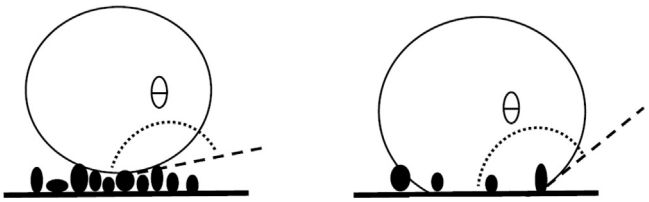

Fig. 10. Schematic description of (a) Cassie–Baxter and (b) Wenzel wetting states.

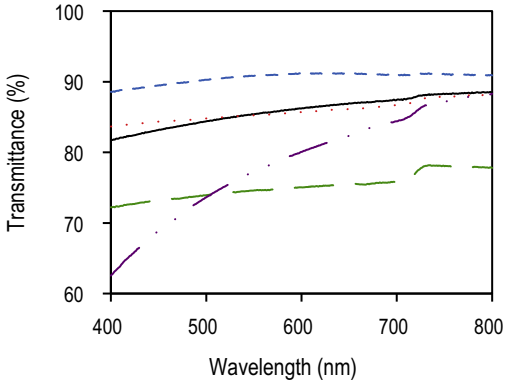

Fig. 11. Comparison of the relative transparencies of uncoated glass slide (———) and TPSC/silica coated glass surfaces by different methods. Doctor blade coating (— —), spin-coating of silica particles on TPSC (·····), spin-coating of TPSC/silica (1/10) (—— ——) and spray coating (—··—··—).

addition, the longer distances between the silica particles in sample S1, when compared to S2 and S3 may result in drop pinning, resulting in a fairly high CAH value.

For various applications a critical requirement is the transparency of the superhydrophobic coatings. We measured the transparencies of the glass slides used as the substrate and TPSC/silica coated glass slides obtained by various coating methods described in this paper. Percent transmittance versus wavelength curves obtained against air as the reference are reproduced in Fig. 11. Uncoated glass slides on the average show 85% transparency in the visible region. It is interesting to note that the doctor blade coated TPSC/silica film, with a thickness of about 5 μm, shows an average of 90% transparency, which is higher than the glass substrate. Silica spin-coated TPSC film with a thickness of about 20 μm, also displays about 85% transparency similar to that of the glass substrate. Spray coated TPSC/silica (1/10) film, with a thickness of about 35 μm displays a fairly low transparency of around 63% at 400 nm, which gradually increases to 85% at 800 nm. Spin coated TPSC/silica (1/10) film has the lowest average transparency of around 75%, which does not change with wavelength. These results indicate that the transparency of the silica modified superhydrophobic TPSC films is fairly good. As might be expected, transparency of the coating depends on the film thickness and the coating method used.

4. Conclusions

Influence of coating methods on the preparation of superhydrophobic silicone–urea copolymer (TPSC) surfaces, modified by the incorporation of hydrophobic fumed silica nanoparticles was investigated. The methods employed were: (i) successive spin coating of hydrophobic fumed silica dispersed in an organic solvent onto preformed silicone–urea films, (ii) spin coating of silica–polymer dispersion onto a glass substrate, (iii) direct coating of silica–polymer mixture by using a doctor blade, onto a glass substrate, and (iv) spray coating of silica–polymer dispersion by an air-brush onto a glass substrate. In addition to the method used, influence of the concentration of the fumed silica dispersion and the number of coating layers applied on the surface topography, the extent and nature of the silica coverage and average surface roughness were determined. All surfaces obtained displayed micro-nano hierarchical structures as observed by SEM studies. It was demonstrated that superhydrophobic surfaces could be obtained by all methods employed, which is clearly indicated by the static and advancing water contact angles well above 150° and contact angle hysteresis values below 10°. Two critical questions regarding the surfaces formed are their durability and transparency. Durability or superhydrophobicity retention of the coated surfaces was determined by two simple tests. First one involved the measurement of the water contact angles (CA) and contact angle hysteresis (CAH) on samples, which were stored for over a year under ambient conditions. In the second test a *scotch tape* was firmly pressed onto the coated surface and was peeled off after 5 s of contact. CA and CAH values did not show any noticeable change after these tests, which indicated the formation of durable, superhydrophobic surfaces. Regarding the transparency of the films, we have demonstrated that superhydrophobic TPSC/silica films with thicknesses up to about 20 μm are very transparent. For many practical applications spray coating provides a simple route for the preparation of superhydrophobic surfaces. On the other hand, doctor blade technique can be used to obtain superhydrophobic polymer films or textiles by using conventional direct coating methods.

References

[1] W. Barthlott, C. Neinhuis, Purity of the sacred lotus, or escape from contamination in biological surfaces, Planta 202 (1) (1997) 1–8.
[2] C. Neinhuis, W. Barthlott, Characterization and distribution of water-repellent, self-cleaning plant surfaces, Ann. Bot. 79 (6) (1997) 667–677.
[3] T. Verho, C. Bower, P. Andrew, S. Franssila, O. Ikkala, R.H.A. Ras, Mechanically durable superhydrophobic surfaces, Adv. Mater. 23 (5) (2011) 673–678.
[4] M. Nosonovsky, B. Bhushan, Superhydrophobic surfaces and emerging applications: non-adhesion, energy, green engineering, Curr. Opin. Colloid Interface Sci. 14 (4) (2009) 270–280.
[5] P.N. Manoudis, I. Karapanagiotis, A. Tsakalof, I. Zuburtikudis, C. Panayiotou, Superhydrophobic composite films produced on various substrates, Langmuir 24 (19) (2008) 11225–11232.
[6] C.Y. Peng, S.L. Xing, Z.Q. Yuan, J.Y. Xiao, C.Q. Wang, J.C. Zeng, Preparation and anti-icing of superhydrophobic PVDF coating on a wind turbine blade, Appl. Surf. Sci. 259 (2012) 764–768.
[7] P.N. Manoudis, I. Karapanagiotis, A. Tsakalof, I. Zuburtikudis, B. Kolinkeova, C. Panayiotou, Surface properties of superhydrophobic coatings for stone protection, J. Nano Res. 8 (2009) 23–33.
[8] L.C. Gao, T.J. McCarthy, The "lotus effect" explained: two reasons why two length scales of topography are important, Langmuir 22 (7) (2006) 2966–2967.
[9] D. Oner, T.J. McCarthy, Ultrahydrophobic surfaces. Effects of topography length scales on wettability, Langmuir 16 (20) (2000) 7777–7782.
[10] B. Bhushan, Y.C. Jung, Natural and biomimetic artificial surfaces for superhydrophobicity, self-cleaning, low adhesion, and drag reduction, Prog. Mater. Sci. 56 (1) (2011) 1–108.
[11] W. Chen, A.Y. Fadeev, M.C. Hsieh, D. Oner, J. Youngblood, T.J. McCarthy, Ultrahydrophobic and ultralyophobic surfaces: some comments and examples, Langmuir 15 (10) (1999) 3395–3399.
[12] N. Takeshita, L.A. Paradis, D. Oner, T.J. McCarthy, W. Chen, Simultaneous tailoring of surface topography and chemical structure for controlled wettability, Langmuir 20 (19) (2004) 8131–8136.
[13] L.C. Gao, T.J. McCarthy, Contact angle hysteresis explained, Langmuir 22 (14) (2006) 6234–6237.
[14] J.W. Krumpfer, T.J. McCarthy, Contact angle hysteresis: a different view and a trivial recipe for low hysteresis hydrophobic surfaces, Faraday Dis. 146 (2010) 103–111.
[15] Y.C. Jung, B. Bhushan, Contact angle, adhesion and friction properties of micro- and nanopatterned polymers for superhydrophobicity, Nanotechnology 17 (19) (2006) 4970–4980.
[16] K. Koch, B. Bhushan, Y.C. Jung, W. Barthlott, Fabrication of artificial Lotus leaves and significance of hierarchical structure for superhydrophobicity and low adhesion, Soft Matter. 5 (7) (2009) 1386–1393.
[17] G. McHale, N.J. Shirtcliffe, M.I. Newton, Contact-angle hysteresis on superhydrophobic surfaces, Langmuir 20 (23) (2004) 10146–10149.
[18] Z.W. He, W. Zhang, W.L. Wang, M. Tassin, J.J. Gu, Q.L. Liu, et al., Fabrication of Fe-wings used for micro imprinting with a natural butterfly wing structure by in situ carbothermic reduction, J. Mater. Chem. B 1 (12) (2013) 1673–1677.

[19] F. Yao, Q.Q. Yang, C. Yin, S.M. Zhu, D. Zhang, W.J. Moon, et al., Biomimetic Bi2WO6 with hierarchical structures from butterfly wings for visible light absorption, Mater. Lett. 77 (2012) 21–24.
[20] G.D. Bixler, B. Bhushan, Rice- and butterfly-wing effect inspired self-cleaning and low drag micro/nanopatterned surfaces in water, oil, and air flow, Nanoscale 6 (1) (2014) 76–96.
[21] G.D. Bixler, A. Theiss, B. Bhushan, S.C. Lee, Anti-fouling properties of microstructured surfaces bio-inspired by rice leaves and butterfly wings, J. Colloid Interface Sci. 419 (2014) 114–133.
[22] G.D. Bixler, B. Bhushan, Bioinspired rice leaf and butterfly wing surface structures combining shark skin and lotus effects, Soft Matter. 8 (44) (2012) 11271–11284.
[23] Y.M. Zheng, X.F. Gao, L. Jiang, Directional adhesion of superhydrophobic butterfly wings, Soft Matter. 3 (2) (2007) 178–182.
[24] T. Wagner, C. Neinhuis, W. Barthlott, Wettability and contaminability of insect wings as a function of their surface sculptures, Acta Zool. 77 (3) (1996) 213–225.
[25] D. Byun, J. Hong, P. Saputra, J.H. Ko, Y.J. Lee, H.C. Park, et al., Wetting characteristics of insect wing surfaces, J. Bionic Eng. 6 (1) (2009) 63–70.
[26] R.N. Wenzel, Resistance of solid surfaces to wetting by water, Ind. Eng. Chem. 28 (1936) 546–551.
[27] A.B.D. Cassie, S. Baxter, Wettability of porous surfaces, Trans. Faraday Soc. 40 (1944) 546–551.
[28] P. Roach, N.J. Shirtcliffe, M.I. Newton, Progess in superhydrophobic surface development, Soft Matter. 4 (2) (2008) 224–240.
[29] T. Onda, S. Shibuichi, N. Satoh, K. Tsujii, Super-water-repellent fractal surfaces, Langmuir 12 (9) (1996) 2125–2127.
[30] C.W. Extrand, Contact angles and hysteresis on surfaces with chemically heterogeneous islands, Langmuir 19 (9) (2003) 3793–3796.
[31] C.W. Extrand, Model for contact angles and hysteresis on rough and ultraphobic surfaces, Langmuir 18 (21) (2002) 7991–7999.
[32] H.Y. Erbil, C.E. Cansoy, Range of applicability of the Wenzel and Cassie-Baxter equations for superhydrophobic surfaces, Langmuir 25 (24) (2009) 14135–14145.
[33] J. Bravo, L. Zhai, Z.Z. Wu, R.E. Cohen, M.F. Rubner, Transparent superhydrophobic films based on silica nanoparticles, Langmuir 23 (13) (2007) 7293–7298.
[34] K. Acatay, E. Simsek, C. Ow-Yang, Y.Z. Menceloglu, Tunable, superhydrophobically stable polymeric surfaces by electrospinning, Angew. Chem. Int. Ed. 43 (39) (2004) 5210–5213.
[35] J.T. Han, X.R. Xu, K.W. Cho, Diverse access to artificial superhydrophobic surfaces using block copolymers, Langmuir 21 (15) (2005) 6662–6665.
[36] Y.Y. Yan, N. Gao, W. Barthlott, Mimicking natural superhydrophobic surfaces and grasping the wetting process: a review on recent progress in preparing superhydrophobic surfaces, Adv. Colloid Interface Sci. 169 (2) (2011) 80–105.
[37] N.J. Shirtcliffe, G. McHale, S. Atherton, M.I. Newton, An introduction to superhydrophobicity, Adv. Colloid Interface Sci. 161 (1–2) (2010) 124–138.
[38] M.L. Ma, R.M. Hill, Superhydrophobic surfaces, Curr. Opin. Colloid Interface Sci. 11 (4) (2006) 193–202.
[39] I. Yilgor, S. Bilgin, M. Isik, E. Yilgor, Tunable wetting of polymer surfaces, Langmuir 28 (41) (2012) 14808–14814.
[40] I. Yilgor, S. Bilgin, M. Isik, E. Yilgor, Facile preparation of superhydrophobic polymer surfaces, Polymer 53 (6) (2012) 1180–1188.
[41] N.J. Shirtcliffe, G. McHale, M.I. Newton, C.C. Perry, P. Roach, Superhydrophobic to superhydrophilic transitions of sol-gel films for temperature, alcohol or surfactant measurement, Mater. Chem. Phys. 103 (1) (2007) 112–117.
[42] L. Zhang, Z.L. Zhou, B. Cheng, J.M. DeSimone, E.T. Samulski, Superhydrophobic behavior of a perfluoropolyether lotus-leaf-like topography, Langmuir 22 (20) (2006) 8576–8580.
[43] P.N. Manoudis, I. Karapanagiotis, A. Tsakalof, I. Zuburtikudis, B. Kolinkeova, C. Panayiotou, Superhydrophobic films for the protection of outdoor cultural heritage assets, Appl. Phys. A Mater. Sci. Process. 97 (2) (2009) 351–360.
[44] N.J. Shirtcliffe, G. McHale, M.I. Newton, The superhydrophobicity of polymer surfaces: recent developments, J. Polym. Sci. B Polym. Phys. 49 (17) (2011) 1203–1217.
[45] HDK – Pyrogenic Silica. Available from: http://www.wacker.com/cms/media/publications/downloads/6180_EN.pdf
[46] L.C. Gao, T.J. McCarthy, A perfectly hydrophobic surface (theta(A)/theta(R) = 180 degrees/180 degrees), J. Am. Chem. Soc. 128 (28) (2006) 9052–9053.
[47] L.C. Gao, T.J. McCarthy, "Artificial lotus leaf" prepared using a 1945 patent and a commercial textile, Langmuir 22 (14) (2006) 5998–6000.
[48] K.A. Wier, T.J. McCarthy, Condensation on ultrahydrophobic surfaces and its effect on droplet mobility: ultrahydrophobic surfaces are not always water repellant, Langmuir 22 (6) (2006) 2433–2436.
[49] L.C. Gao, T.J. McCarthy, Ionic liquids are useful contact angle probe fluids, J. Am. Chem. Soc. 129 (13) (2007) 3804+.
[50] L.C. Gao, T.J. McCarthy, How Wenzel and Cassie were wrong, Langmuir 23 (7) (2007) 3762–3765.
[51] J.A. Lee, T.J. McCarthy, Polymer surface modification: topography effects leading to extreme wettability behavior, Macromolecules 40 (11) (2007) 3965–3969.
[52] L.C. Gao, A.Y. Fadeev, T.J. McCarthy, Superhydrophobicity and contact-line issues, MRS Bull. 33 (8) (2008) 747–751.
[53] L.C. Gao, T.J. McCarthy, Teflon is hydrophilic, comments on definitions of hydrophobic, shear versus tensile hydrophobicity, and wettability characterization, Langmuir 24 (17) (2008) 9183–9188.
[54] L.C. Gao, T.J. McCarthy, (CH3)(3)SiCl/SiCl4 azeotrope grows superhydrophobic nanofilaments, Langmuir 24 (2) (2008) 362–364.
[55] L.C. Gao, T.J. McCarthy, Wetting 101 degrees, Langmuir 25 (24) (2009) 14105–14115.
[56] J.W. Krumpfer, P. Bian, P.W. Zheng, L.C. Gao, T.J. McCarthy, Contact angle hysteresis on superhydrophobic surfaces: an ionic liquid probe fluid offers mechanistic insight, Langmuir 27 (6) (2011) 2166–2169.
[57] J.W. Krumpfer, T.J. McCarthy, Dip-coating crystallization on a superhydrophobic surface: a million mounted crystals in a 1 cm(2) array, J. Am. Chem. Soc. 133 (15) (2011) 5764–5766.
[58] M. McCarthy, K. Gerasopoulos, R. Enright, J.N. Culver, R. Ghodssi, E.N. Wang, Biotemplated hierarchical surfaces and the role of dual length scales on the repellency of impacting droplets, Appl. Phys. Lett. 100 (26) (2012) 263701–263705.
[59] B. Bhushan, Y.C. Jung, Micro- and nanoscale characterization of hydrophobic and hydrophilic leaf surfaces, Nanotechnology 17 (11) (2006) 2758–2772.
[60] M. Nosonovsky, B. Bhushan, Biomimetic superhydrophobic surfaces: multiscale approach, Nano Lett. 7 (9) (2007) 2633–2637.
[61] M. Nosonovsky, B. Bhushan, Biologically inspired surfaces: broadening the scope of roughness, Adv. Funct. Mater. 18 (6) (2008) 843–855.
[62] B. Bhushan, Biomimetics: lessons from nature – an overview, Philos. Trans. R. Soc. Math. Phys. Eng. Sci. 367 (1893) (2009) 1445–1486.
[63] K. Koch, B. Bhushan, W. Barthlott, Multifunctional surface structures of plants: an inspiration for biomimetics, Prog. Mater. Sci. 54 (2) (2009) 137–178.
[64] P. Wagner, R. Furstner, W. Barthlott, C. Neinhuis, Quantitative assessment to the structural basis of water repellency in natural and technical surfaces, J. Exp. Bot. 54 (385) (2003) 1295–1303.
[65] K. Koch, C. Neinhuis, H.J. Ensikat, W. Barthlott, Self assembly of epicuticular waxes on living plant surfaces imaged by atomic force microscopy (AFM), J. Exp. Bot. 55 (397) (2004) 711–718.
[66] R. Furstner, W. Barthlott, C. Neinhuis, P. Walzel, Wetting and self-cleaning properties of artificial superhydrophobic surfaces, Langmuir 21 (3) (2005) 956–961.
[67] K. Koch, K.D. Hartmann, L. Schreiber, W. Barthlott, C. Neinhuis, Influences of air humidity during the cultivation of plants on wax chemical composition, morphology and leaf surface wettability, Environ. Exp. Bot. 56 (1) (2006) 1–9.
[68] H.J. Ensikat, P. Ditsche-Kuru, C. Neinhuis, W. Barthlott, Superhydrophobicity in perfection: the outstanding properties of the lotus leaf, Beilstein J. Nanotechnol. 2 (2011) 152–161.
[69] N.J. Shirtcliffe, G. McHale, M.I. Newton, C.C. Perry, Intrinsically superhydrophobic organosilica sol-gel foams, Langmuir 19 (14) (2003) 5626–5631.
[70] G. McHale, S. Aqil, N.J. Shirtcliffe, M.I. Newton, H.Y. Erbil, Analysis of droplet evaporation on a superhydrophobic surface, Langmuir 21 (24) (2005) 11053–11060.
[71] N.J. Shirtcliffe, G. McHale, M.I. Newton, C.C. Perry, P. Roach, Porous materials show superhydrophobic to superhydrophilic switching, Chem. Commun. 25 (2005) 3135–3137.
[72] G. McHale, D.L. Herbertson, S.J. Elliott, N.J. Shirtcliffe, M.I. Newton, Electrowetting of nonwetting liquids and liquid marbles, Langmuir 23 (2) (2007) 918–924.
[73] G. McHale, M.I. Newton, N.J. Shirtcliffe, Dynamic wetting and spreading and the role of topography, J. Phys. Condens. Matter. 21 (46) (2009) 464122–464133.
[74] N.J. Shirtcliffe, G. McHale, M.I. Newton, Learning from superhydrophobic plants: the use of hydrophilic areas on superhydrophobic surfaces for droplet control, Langmuir 25 (24) (2009) 14121–14128.
[75] L. Feng, S.H. Li, Y.S. Li, H.J. Li, L.J. Zhang, J. Zhai, et al., Super-hydrophobic surfaces: from natural to artificial, Adv. Mater. 14 (24) (2002) 1857–1860.
[76] C. Kosak Söz, E. Yilgör, I. Yilgör, Influence of the average surface roughness on the formation of superhydrophobic polymer surfaces through spin-coating with hydrophobic fumed silica, Polymer 62 (2015) 118–128.